Polyhedron 200 (2021) 115130

Contents lists available at ScienceDirect

Polyhedron

journal homepage: www.elsevier.com/locate/poly

Synthesis, characterization, X-ray crystallography analysis and cell viability study of (η^6-*p*-cymene)Ru(NH_2R)X_2 (X = Cl, Br) derivatives

Sarah L. McDarmont [a], Meredith H. Jones [b], Colin D. McMillen [c], Everett Clinton Smith [d], Jared A. Pienkos [a], Evan E. Joslin [b,*]

[a] The University of Tennessee at Chattanooga, Department of Chemistry & Physics, 615 McCallie Avenue, Chattanooga, TN 37403, USA
[b] Department of Chemistry, The University of the South, Sewanee, TN 37383, USA
[c] Clemson University, Department of Chemistry, Clemson, SC 29634, USA
[d] Department of Biology, The University of the South, Sewanee, TN 37383, USA

ARTICLE INFO

Article history:
Received 13 January 2021
Accepted 22 February 2021
Available online 6 March 2021

Keywords:
Coordination chemistry
Ruthenium(II) complexes
X-ray crystallography

ABSTRACT

Studies over the past few decades demonstrate the potential for metallodrugs as bioactive therapeutics. Here, we describe six new ruthenium(II) complexes with the general motif of (η^6-*p*-cymene)Ru(NH_2R)X_2, where NH_2R is either the influenza A antiviral drugs rimantadine or amantadine or the *N*-methyl-D-aspartate [NMDA] receptor antagonist, memantine and X = Cl or Br. All complexes were synthesized in high yield and purity and characterized by NMR spectroscopy and X-ray crystallography. Both the chlorine and bromine ruthenium(II) *p*-cymene complexes demonstrated cellular toxicity profiles similar to their respective free ligand, indicating that complexation to ruthenium(II) centers does not significantly increase toxicity of the bioactive ligand.

1. Introduction

Transition metal complexes have recently gained interest for their therapeutic potential [1]. One of the best known examples is the platinum(II) salt cisplatin, which is commonly used as a treatment for cancer [2]. More recently, gold complexes have been investigated as anti-cancer agents, and have shown promising results in clinical trials [3]. In addition to these precious metal species, piano stool ruthenium(II) arene complexes have shown promise as chemotherapeutics and antimalarial drugs. Specific examples include RAPTA-C [4] and (η^6-*p*-cymene)Ru(CQ)Cl_2 (CQ = chloroquine) (Fig. 1) [5]. In particular, ruthenium-complexed CQ was considerably more potent than free CQ against CQ-resistant *Plasmodium falciparum*, suggesting that derivatization of existing FDA-approved therapeutics is a promising approach for some compounds [5].

This strategy of attaching a bioactive ligand directly to the metal center has been employed for the generation of antivirals. For instance, Neamati et al. explored the bioactivity of the HIV-1 integrase inhibitor analogs of diketo acid (DKA) and Elvitegravier (EVG) bound to a (η^6-*p*-cymene)ruthenium(II) fragment and found that the ruthenium(II) complexes were less active than the corresponding free ligands (Fig. 1) [6]. Whereas, similarly structured bis-chelate complexes with magnesium(II), manganese(II), cobalt (II), and zinc(II) with similar ligands have shown similar or better HIV-1 inhibition profiles when compared to the free ligands [7]. More recently, an amantadine (ATN) Cu (II) complex, {[$ATNH^+$][$CuCl_3$]}$_n$, was evaluated against a series of ATN-resistant influenza A virus strains. This copper(II) complex was able to inhibit influenza A virus strains that are not inhibited by amantadine or other adamantane derivatives [8].

In a recent perspective article, amantadine and its derivatives (e.g., memantine and rimantadine) were suggested as potential treatments for COVID-19 [9]. Though amantadine targets the influenza A virus M2 proton-specific ion channel (M2) [10], the coronavirus envelope (E) protein could also function as an ion channel [11]. Despite variable antiviral activity of amantadine, memantine, and rimantadine against human and animal coronaviruses [12–17], derivatization of these biologically active ligands to transition metals could increase efficacy. Therefore, due to the biological activity of amantadine [18], memantine (*N*-methyl-D-aspartate [NMDA] receptor antagonist) [19], rimantadine (active against influenza A virus) [20], and the well documented synthesis of ruthenium(II) arene complexes, we envisioned the synthesis of (η^6-*p*-cymene) ruthenium(II) complexes that contain these ligands. Indeed, the structural literature contains a number of complexes of ruthenium(II) chloride with extended amines bound opposite a *p*-cym-

* Corresponding author.
E-mail address: eejoslin@sewanee.edu (E.E. Joslin).

https://doi.org/10.1016/j.poly.2021.115130
0277-5387/

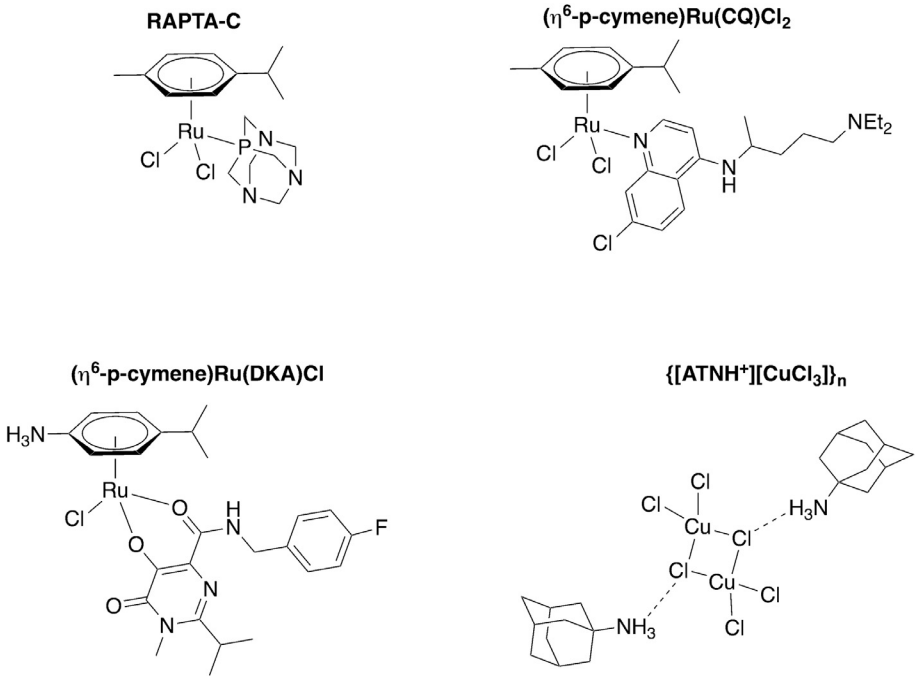

Fig. 1. Some biologically active inorganic compounds (ATN = amantadine).

ene group, including aniline [21], 4-methylaniline [21,22], benzylamine [23], 2,6-diisopropylaniline [24], *p*-toluidine [25], and 2,6-bis(diphenylmethyl)-4-methylaniline [26], as examples somewhat related to the target amantadine, memantine, and rimantadine that do not have additional traditional hydrogen bonding donor or acceptor groups on the amine ligand. The structures of related dibromide complexes of ruthenium(II) with *p*-cymene and extended amines are, to our knowledge, not reported in the literature. Herein, we report the synthesis and characterization of these derivatives and their effect on cell viability. Both the chlorine and bromine (η^6-*p*-cymene)ruthenium(II) complexes demonstrated cellular toxicity profiles similar to their respective free ligand, indicating that the presence of a ruthenium(II) center does not significantly impact cellular toxicity. Overall, all complexes had 50% cytotoxic concentrations (CC_{50}) above 100 μM, providing a suitable concentration window for future antiviral testing in cell culture.

2. Material and methods

2.1. General methods

Unless otherwise noted, all synthetic procedures were performed under anaerobic conditions in a nitrogen-filled glovebox or by using standard Schlenk techniques. ^{1}H NMR, and $^{13}C\{^1H\}$ NMR (operating frequency 125 MHz) spectra were recorded on a JOEL ECS or JOEL ECX 400 MHz spectrometer. All ^{1}H and $^{13}C\{^1H\}$ NMR spectra are referenced against residual proton signals (^{1}H NMR) or the ^{13}C resonances of the deuterated solvent (^{13}C NMR). $[(\eta^6\text{-}p\text{-cy})RuBr_2]_2$ was synthesized according to a previously reported procedure [27]. All other reagents were obtained from a commercial source and used as received unless otherwise indicated. All solvents were purchased as anhydrous solvents and used as received.

2.2. X-ray crystallography

Single crystal X-ray diffraction data was obtained on complexes **1**–**6** using crystals mounted on low background cryogenic loops with paratone oil. Data were collected under nitrogen at 100 K using a Bruker D8 Venture diffractometer with a Mo Kα (λ = 0.71073 Å) microfocus source and a Photon 2 detector. Diffraction images were collected in 0.5° increments using phi and omega scans. Instrument control, data processing, and scaling were performed through the Apex 3 software suite (SAINT and SADABS routines) [28]. Symmetry analysis, structure solution, and structure refinement were performed through the SHELXTL suite (XPREP, SHELXT, and SHELXL routines) [29]. Structure refinement was performed by full-matrix least squares techniques on F^2. All non-hydrogen atoms were refined anisotropically. Hydrogen atoms attached to carbon atoms were modeled in idealized locations using appropriate riding models. The amine hydrogen atoms were identified from the difference electron density maps and fully refined. Crystallographic data for complexes **1**–**6** is given in Table 1. Additionally, a chloroform solvate of complex **2**, **2**·2$CHCl_3$, was obtained by allowing the chloroform/pentane system to evaporate to dryness. Crystallographic data and structural figures of this solvated species are provided in the SI.

2.3. Viability measurements

DBT-9 (delayed brain tumor, murine astrocytoma clone 9) cells [30] were maintained at 37 °C and 5% CO_2 in Dulbecco's modified Eagle's medium (DMEM) supplemented with 10% horse serum, 100 U/mL penicillin and streptomycin, and 10 mM HEPES. For viability studies, DBT-9 cells were plated into opaque tissue culture-treated 96-well plates at 20,000 cells/well approximately 24 h prior to complex addition. Complexes were diluted to either 25 mM (complexes **3**,**6**) or 100 mM (complexes **1**,**2**,**4**,**5**) in DMSO. Serial two-fold dilutions were generated in DMSO ranging from 100 mM to 0.098 mM. Complexes were diluted into DMEM at 1:1000 (100 μM to 0.098 μM); the final concentration of DMSO was 0.4% (v/v) across all dilutions. Concentrations higher than 100 μM were not attempted, as DMSO can begin to affect cell viability at or above 0.5% (v/v). DMEM was removed from all wells, and 100 μL of DMEM containing the indicated concentration of complex or vehicle [0.4% (v/v) DMSO] was added. There were four

Table 1
Crystallographic Data for Complexes **1**–**6**.

	1	2	3	4	5	6
Empirical formula	$C_{20}H_{31}Cl_2NRu$	$C_{22}H_{35}Cl_2NRu$	$C_{22}H_{35}Cl_2NRu$	$C_{20}H_{31}Br_2NRu$	$C_{22}H_{35}Br_2NRu$	$C_{22}H_{35}Br_2NRu$
F. W. (g/mol)	457.43	485.48	485.48	546.35	574.40	574.40
Crystal system	triclinic	monoclinic	tetragonal	triclinic	triclinic	monoclinic
Space group	*P*-1	$P2_1/c$	*I*-4	*P*-1	*P*-1	$P2_1/c$
a (Å)	7.2756(15)	11.4061(7)	26.109(3)	7.3713(5)	7.8760(6)	6.7600(4)
b (Å)	11.620(2)	15.9222(10)	26.109(3)	11.7060(8)	11.8014(9)	27.8682(17)
c (Å)	12.714(3)	12.7305(7)	6.4437(11)	13.1021(9)	13.4882(11)	36.107(2)
α (°)	71.013(8)	90	90	69.288(2)	65.487(3)	90
β (°)	77.478(7)	110.927(2)	90	76.888(2)	76.608(3)	90.824(2)
γ (°)	79.387(7)	90	90	76.047(2)	85.685(3)	90
Volume ($Å^3$)	984.7(4)	2159.5(2)	4392.5(13)	1013.73(12)	1109.37(15)	6801.4(7)
Z	2	4	8	2	2	12
D (calcd)(g/cm^3)	1.543	1.493	1.468	1.790	1.720	1.683
μ, mm^{-1}	1.069	0.980	0.964	4.717	4.315	4.223
θ range,°	2.13–28.38	2.56–28.49	2.21–25.24	2.10–28.50	3.02–30.57	2.26–26.00
Reflections coll.	46,548	51,758	21,878	47,954	60,475	92,444
Indep. reflections	4914	5467	3973	5126	6763	13,385
R(int)	0.0445	0.0279	0.0860	0.0290	0.0346	0.0456
No. of parameters	228	248	240	228	248	733
No. of restraints	0	0	72	0	0	0
R indices	R_1 = 0.0178	R_1 = 0.0168	R_1 = 0.0900	R_1 = 0.0143	R_1 = 0.0165	R_1 = 0.0299
(I greater than 2σ(I))	wR_2 = 0.0404	wR_2 = 0.0399	wR_2 = 0.1860	wR_2 = 0.0320	wR_2 = 0.0391	wR_2 = 0.0656
R indices	R_1 = 0.0207	R_1 = 0.0186	R_1 = 0.0952	R_1 = 0.0159	R_1 = 0.0179	R_1 = 0.0391
(all data)	wR_2 = 0.0424	wR_2 = 0.0418	wR_2 = 0.1885	wR_2 = 0.0327	wR_2 = 0.0408	wR_2 = 0.0700
Goodness of fit	1.094	1.068	1.120	1.077	1.066	1.027
Largest diff. peak/hole ($e/Å^3$)	0.506/-0.465	0.444/-0.484	1.435/-1.782	0.445/-0.461	0.488/-0.703	1.812/-0.988
CCDC deposition no.	2,055,507	2,055,508	2,055,509	2,055,510	2,055,511	2,055,512

biological replicates for each concentration of complex. Cells were cultured as described above for 24 h post-addition. Viability was determined using CellTiter-Glo according to manufacturer's instructions, and luminescence was measured using a BioTek Synergy HTX plate reader using a two-second integration time. All graphs were generated using GraphPad Prism 9. All data were normalized from 0% to 100% using GraphPad Prism 9. There was no statistical difference between vehicle [0.4% (v/v) DMSO] and the lowest concentration of each complex (0.098 μM). The box and whisker plots represent all four biological replicates for each concentration, and none were removed during data processing and analysis.

2.4. Synthesis

2.4.1. Synthesis of (*p*-cy)Ru(amantadine)Cl_2 (1)

$[(\eta^6\text{-}p\text{-cy})RuCl_2]_2$ (500 mg, 0.816 mmol) was dissolved in chloroform (15 mL). To this, a solution of amantadine (284 mg, 1.89 mmol) in chloroform (5 mL) was added dropwise. The solution turned bright orange-red, and after 45 min, the solution was slowly added to stirring hexanes (40 mL). An orange precipitate formed and was collected on a fine-porosity frit and washed with hexanes. The solid was dried in vacuo to yield a bright orange solid (510 mg, 68% yield). Orange-red block-like crystals were obtained by layering a chloroform solution of the complex with pentane. ^{1}H NMR (400 MHz, $CDCl_3$) δ 5.53 (d, $^3J_{HH}$ = 6.0 Hz, 2H, *p*-cy: C*H*), 5.46 (d, $^3J_{HH}$ = 6 Hz, 2H, *p*-cy: C*H*), 3.04 (sept, $^3J_{HH}$ = 7 Hz, 1H, *p*-cy: C*H*$(CH_3)_2$, 2.56 (s, 2H, N*H*$_2$), 2.26 (s, 3H, *p*-cy-C*H*$_3$), 2.13 (m, 3H, amantadine), 1.82 – 1.50 (m, 12H, amantadine), 1.28 (d, $^3J_{HH}$ = 7 Hz, 6H, CH(C*H*$_3$)$_2$). ^{13}C NMR (101 MHz, $CDCl_3$) δ 103.02 (ispo-C of *p*-cy), 95.41 (*ipso-C* of *p*-cy), 81.32 (*C*H-*p*-cy), 79.54 (*C*H-*p*-cy), 53.51, 44.53, 36.01, 29.62 (amantadine), 30.76 (*C*H$(CH_3)_2$ of *p*-cy), 22.25 (CH(*C*H$_3$)$_2$ of *p*-cy), 18.90 (*C*H$_3$ of *p*-cy). Anal. Calc'd. for $C_{20}H_{31}Cl_2NRu$: C, 52.51; H, 6.83; N, 3.06 Found: C, 52.21; H, 6.74; N, 3.14.

2.4.2. Synthesis of (*p*-cy)Ru(memantine)Cl_2 (2)

Memantine•HCl (212 mg, 0.001 mol) was dissolved in RO water (5 mL). KOH was added until the pH was greater than 12. After 40 min, dichloromethane (10 mL) was added and the organic layer was isolated. The aqueous layer was extracted with dichloromethane (2 × 20 mL). The organic portions were combined and dried with $MgSO_4$ and the solvent was removed in vacuo to yield memantine as a yellow oil (109 mg, 62% yield). Under nitrogen, $[(\eta^6\text{-}p\text{-cy})RuCl_2]_2$ (128 mg, 0.209 mmol) was dissolved in chloroform (6 mL) and stirred. To this, a solution of memantine (109 mg, 0.608 mmol) in chloroform (2 mL) was slowly added. After 30 min, the reaction solution was added to pentane (50 mL). The resulting orange precipitate was collected on a fine porosity frit and dried in vacuo (168 mg, 83% yield). Orange block-like crystals were obtained by layering a chloroform solution of the complex with hexanes. ^{1}H NMR (400 MHz, $CDCl_3$) δ 5.49 (d, $^3J_{HH}$ = 5.8 Hz, 2H, *p*-cy: C*H*), 5.45 (d, $^3J_{HH}$ = 5.8 Hz, 2H, *p*-cy: C*H*), 3.05 (sept, $^3J_{HH}$ = 6.9 Hz, 1H, C*H*$(CH_3)_2$), 2.58 (s, 2H, N*H*$_2$), 2.26 (s, 3H, *p*-cy: C*H*$_3$), 2.21 (m, 1H, memantine), 1.66–1.02 (m, 12H,

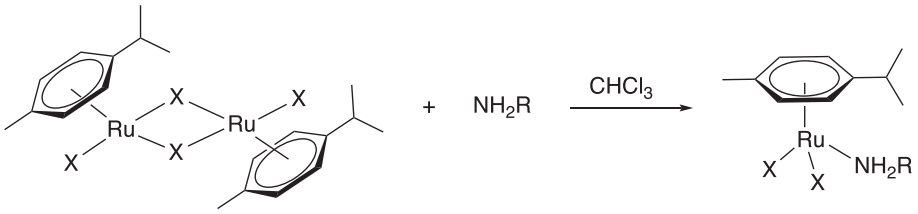

Scheme 1. General Synthesis of (η^6-*p*-cy)Ru(NH_2R)X_2 Complexes.

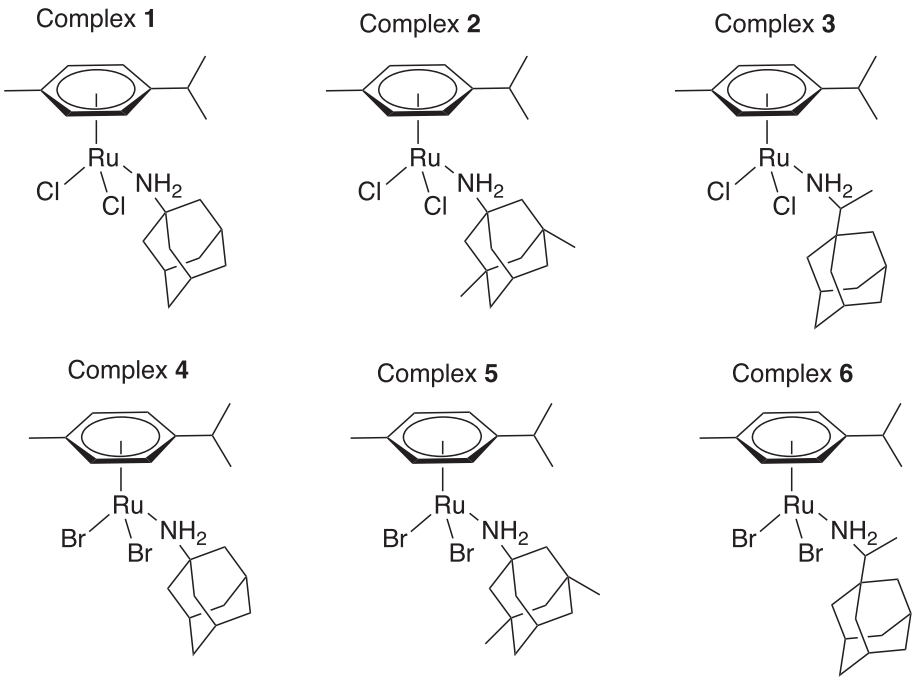

Fig. 2. Ruthenium(II) complexes **1**–**6**.

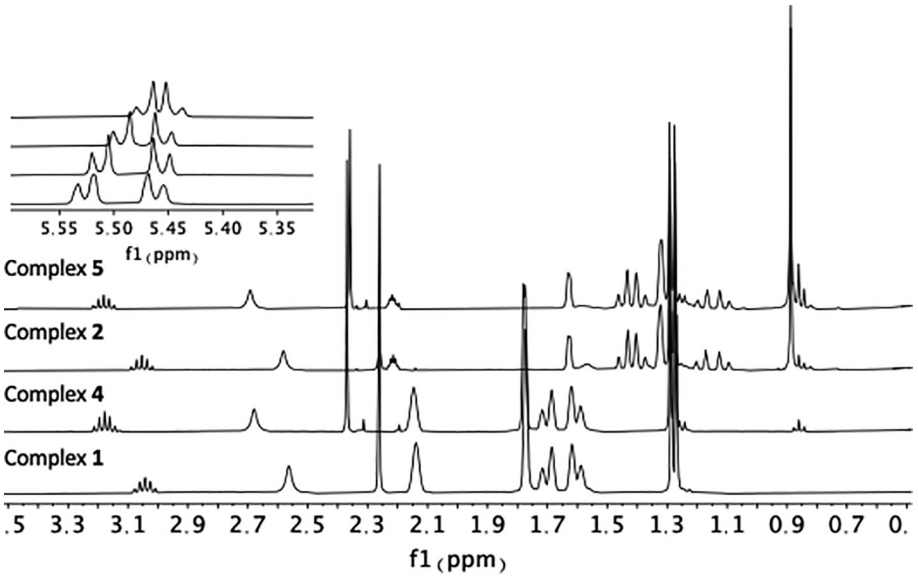

Fig. 3. ^{1}H NMR spectrum of (*p*-cy)Ru(amantadine)Cl_2 (**1**), (*p*-cy)Ru(amantadine)Br_2 (**4**), (*p*-cy)Ru(memantine)Cl_2 (**2**), and (*p*-cy)Ru(memantine)Br_2 (**5**) in $CDCl_3$.

memantine), 1.30 (d, $^{3}J_{HH}$ = 7.0 Hz, 6H, CH(CH_3)$_2$), 0.89 (s, 6H, memantine). ^{13}C NMR (101 MHz, $CDCl_3$) δ 103.38 (ispo-*C* of *p*-cy), 94.94 (*ipso-C* of *p*-cy), 81.67 (*C*H-*p*-cy), 79.17 (*C*H-p-cy), 55.07, 50.66, 50.32, 43.05, 42.36, 32.98, 30.77, 30.38 (memantine), 30.10 (*C*H(CH$_3$)$_2$ of *p*-cy), 22.17 (CH(*C*H$_3$)$_2$ of *p*-cy), 18.78 (*C*H$_3$ of *p*-cy). Anal. Calc'd. for $C_{22}H_{35}Cl_2NRu$: C, 54.43; H, 7.27; N, 2.89 Found: C, 54.43; H, 7.12; N, 2.89.

2.4.3. Synthesis of (p-cy)Ru(rimantadine)Cl_2 (3)

Rimantadine•HCl (202 mg, 0.936 mmol) was dissolved in water (5 mL), and KOH was added until the pH was greater than 12. After stirring for 30 min, dichloromethane (10 mL) was added and the organic layer was collected. The aqueous layer was extracted with dichloromethane (2 × 20 mL). The organic portions were combined and dried with $MgSO_4$ and the solvent was removed in vacuo to yield the rimantadine as a colorless oil (117 mg, 0.653 mmol). Under nitrogen, a solution of rimantadine in chloroform (6 mL) was slowly added to a stirring solution of [(η^6-*p*-cy)$RuCl_2$]$_2$ (133 mg, 0.216 mmol) in chloroform (2 mL). After stirring for 45 min, the reaction was added to hexanes (20 mL) to induce a precipitate. The resulting precipitate was collected on a frit and washed with hexanes to yield an orange solid (156 mg, 72% yield). Orange columnar crystals were obtained by layering a dichloromethane solution of the complex with hexanes. ^{1}H NMR (400 MHz, $CDCl_3$) δ 5.43 (d, $^{3}J_{HH}$ = 5.7 Hz, 1H, *p*-cy: C*H*), 5.29 (d, $^{3}J_{HH}$ = 6.5 Hz, 1H, *p*-cy: C*H*), 5.28 (d, $^{3}J_{HH}$ = 6.6, 1H, *p*-cy: C*H*), 5.16 (d, $^{3}J_{HH}$ = 6.1 Hz, 1H, *p*-cy: C*H*), 3.20 (d, $^{3}J_{HH}$ = 10.3 Hz, 1H, NH_2), 3.03 (sept, $^{3}J_{HH}$ = 7.0 Hz, 1H, *p*-cy: C*H*(CH$_3$)$_2$), 2.70 (m, 1H,

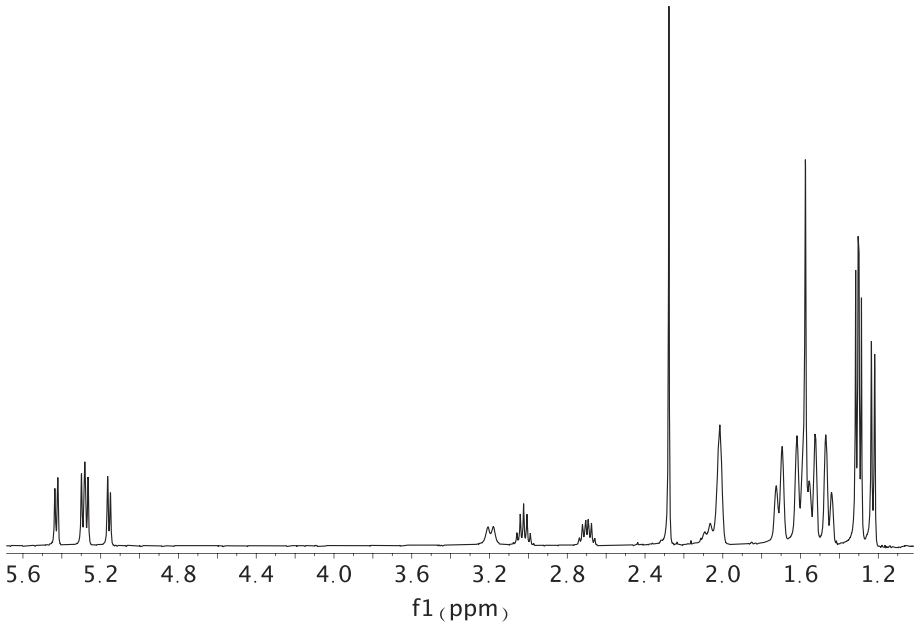

Fig. 4. ^{1}H NMR of (*p*-cy)Ru(rimantadine)Cl_2 (**3**) in $CDCl_3$.

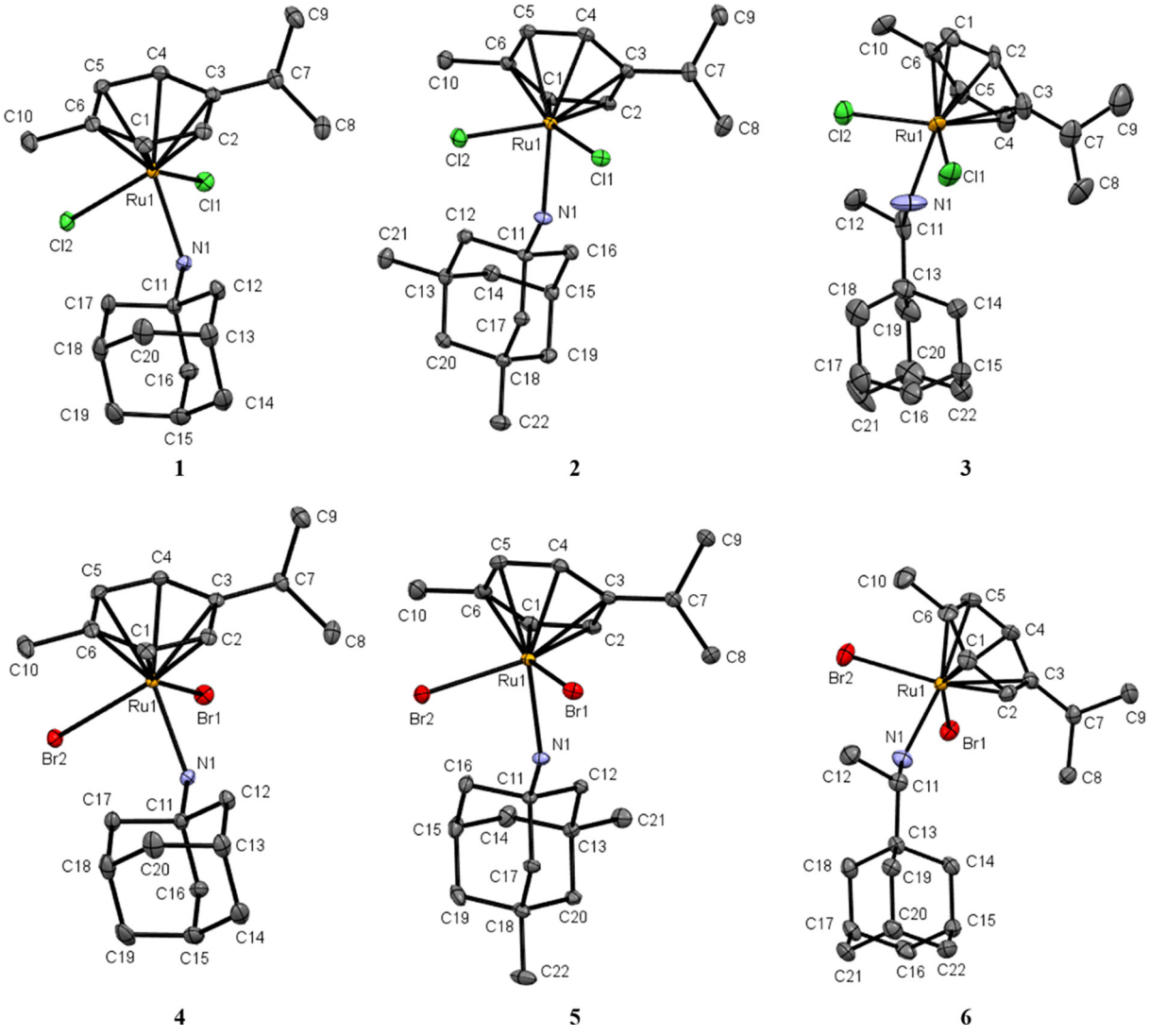

Fig. 5. Structures of complexes **1**–**6** shown as 50% probability ellipsoids (hydrogen atoms omitted for clarity). The structure of complex **6** contains three unique molecules in the asymmetric unit; only one is shown here for simplicity.

rimantadine), 2.28 (s, 3H, *p*-cy: CH_3), 2.09 (m, 1H, NH_2), 2.02 (s, 3H, rimantadine), 1.79 – 1.40 (m, 12H, rimantadine), 1.30 (dd, $^3J_{HH}$ = 6.9, 4.9 Hz, 6H, CH(CH_3)$_2$), 1.23 (d, $^3J_{HH}$ = 6.6 Hz, 3H, rimantadine). ^{13}C NMR (101 MHz, $CDCl_3$) δ 102.6 (*ipso-C* of *p*-cy), 96.0 (*ipso-C* of *p*-cy), 81.9 (*C*H-*p*-cy), 81.6 (*C*H-*p*-cy), 81.2 (*C*H-*p*-cy), 78.9 (*C*H-*p*-cy), 63.7, 38.1, 36.9, 36.7, 28.2, 13.7 (rimantadine), 30.9 (*C*H(CH$_3$)$_2$), 23.0 (CH(*C*H$_3$)$_2$), 21.7 (CH(*C*H$_3$)$_2$), 18.9 (*C*H$_3$of *p*-cy). Anal. Calc'd. for $C_{22}H_{35}Cl_2NRu{\cdot}0.5H_2O$: C, 53.44; H, 7.34; N, 2.83 Found: C, 53.39; H, 7.21; N, 2.90.

2.4.4. Synthesis of (p-cy)Ru(amantadine)Br$_2$ (4)

[(η^6-*p*-cy)RuBr$_2$]$_2$ (500 mg, 0.633 mmol) was dissolved in $CHCl_3$ (15 mL) in a round bottom flask. A solution of amantadine (220 mg, 1.45 mmol) in $CHCl_3$ (5 mL) and added dropwise to the stirring Ru-solution. The solution turned dark orange-red, and after 45 min, the solution was slowly added to stirring hexanes (40 mL). A bright orange precipitate formed and was collected on a fine-porosity frit and washed with hexanes. The solid was in vacuo to yield a bright orange solid (543 mg, 79% yield). Orange columnar crystals were obtained by layering a chloroform solution of the complex with hexanes and pentane. ^{1}H NMR (400 MHz, $CDCl_3$) δ 5.51 (d, $^3J_{HH}$ = 6.0 Hz, 2H, *p*-cy:C*H*), 5.45 (d, $^3J_{HH}$ = 6.0 Hz, 2H, *p*-cy:C*H*), 3.16 (sept, $^3J_{HH}$ = 7.0 Hz, 1H, *p*-cy:C*H*(CH$_3$)$_2$), 2.67 (s, 2H, NH_2), 2.36 (s, 3H, *p*-cy-CH_3), 2.14 (m, 3H, amantadine), 1.83 – 1.53 (m, 12H, amantadine), 1.27 (d, $^3J_{HH}$ = 7.0 Hz, 6H, CH(CH_3)$_2$). ^{13}C NMR (101 MHz, $CDCl_3$) δ 103.91 (ispo-*C* of *p*-cy), 95.75 (*ipso-C* of *p*-cy), 81.14 (*C*H-*p*-cy), 79.09 (*C*H-*p*-cy), 53.99, 44.64, 44.63, 35.96, 29.61 (amantadine) 31.19 (*C*H(CH$_3$)$_2$ of *p*-cy),), 22.32 (CH (*C*H$_3$)$_2$ of *p*-cy), 19.77 (*C*H$_3$ of *p*-cy). Anal. Calc'd. for $C_{20}H_{31}Br_2NRu$: C, 43.97; H, 5.72; N, 2.56 Found: C, 44.03; H, 5.88; N, 2.57.

2.4.5. Synthesis of (p-cy)Ru(memantine)Br$_2$ (5)

Memantine•HCl (217 mg, 1.00 mmol) was dissolved in RO water (5 mL). KOH was added until the pH was greater than 12. After 40 min, dichloromethane (10 mL) was added and the organic layer removed. The aqueous layer was extracted with dichloromethane (2 × 20 mL). The organic portions were combined, dried with $MgSO_4$, and the solvent was removed in vacuo to yield the memantine as a yellow oil (75 mg, 42% yield). Under nitrogen, [(η^6-*p*-cy)RuBr$_2$]$_2$ (110 mg, 0.139 mmol) was dissolved in chloroform (6 mL). To this, a solution of memantine (75.0 mg, 0.418 mmol) in chloroform (2 mL) was slowly added to the stirring solution of [(η^6-*p*-cy)RuBr$_2$]$_2$. After 30 min, the reaction mixture was added to pentane (50 mL), which produced a precipitate. The orange solid was collected on a fine porosity frit and dried in vacuo (92.5 mg, 61% yield). Orange-red tabular crystals were obtained by layering a dichloromethane solution of the complex with hexanes and pentane. ^{1}H NMR (400 MHz, $CDCl_3$) δ 5.50 (d, $^3J_{HH}$ = 5.8 Hz, 2H, p-cy: C*H*), 5.46 (d, $^3J_{HH}$ = 5.8 Hz, 2H, p-cy: C*H*), 3.18 (sept, $^3J_{HH}$ = 6.9 Hz, 1H, C*H*(CH$_3$)$_2$), 2.69 (s, 2H, NH_2), 2.36 (s, 3H, p-cy: CH_3), 2.21 (m, 1H, memantine), 1.63–1.02 (m, 12H, memantine), 1.30 (d, $^3J_{HH}$ = 6.9 Hz 6H, CH(CH_3)$_2$), 0.89 (s, 6H, memantine). ^{13}C NMR (101 MHz, $CDCl_3$) δ 104.32 (ispo-*C* of p-cy), 95.32 (ispo-*C* of *p*-cy), 81.49 (*C*H-*p*-cy), 78.75 (*C*H-*p*-cy) , 55.56, 50.86, 50.28, 43.09, 42.35, 33.03, 31.25, 30.39, 30.10 (memantine), 22.27 (*C*H (CH$_3$)$_2$ of *p*-cy), 19.66 (CH(*C*H$_3$)$_2$ of *p*-cy), 14.17 (*C*H$_3$ of *p*-cy). Anal. Calc'd. for $C_{22}H_{35}Br_2NRu$: C, 46.00; H, 6.14; N, 2.44 Found: C, 46.20; H, 6.14; N, 2.45

2.4.6. Synthesis of (p-cy)Ru(rimantadine)Br$_2$ (6)

Rimantadine•HCl (101 mg, 0.466 mmol) was dissolved in water (5 mL), and KOH was added until the pH was greater than 12. After 30 min, dichloromethane (10 mL) was added and the organic layer was removed. The aqueous layer was extracted with dichloromethane (2 × 20 mL). The organic portions were combined, dried with $MgSO_4$, and the solvent was removed in vacuo to yield rimantadine as a colorless oil (76.0 mg, 92% yield). Under nitrogen, a solution of rimantadine (76.0 mg, 0.424 mmol) in chloroform (3 mL) was slowly added to a stirring solution of [(η^6-*p*-cy)RuBr$_2$]$_2$ (100 mg, 0.127 mmol) in chloroform (5 mL). After stirring for 45 min, the reaction was added to hexanes (20 mL) to induce a precipitate which was collected on a frit and washed with hexanes to yield an orange solid (99.0 mg, 66% yield). Orange-red columnar crystals were obtained by layering a chloroform solution of the complex with hexanes. ^{1}H NMR (400 MHz, $CDCl_3$) δ 5.43 (d, $^3J_{HH}$ = 6.0 Hz, 1H, *p*-cy: C*H*), 5.26 (d, $^3J_{HH}$ = 6.8 Hz, 2H, *p*-cy: C*H*), 5.18 (d, $^3J_{HH}$ = 5.8 Hz, 1H, *p*-cy: C*H*), 3.33 (d, $^3J_{HH}$ = 11.0 Hz, 1H, NH_2), 3.14 (sept, $^3J_{HH}$ = 6.9 Hz, 1H, *p*-cy: C*H*(CH$_3$)$_2$), 2.68 (m, 1H, rimantadine), 2.38 (s, 3H, *p*-cy: CH_3), 2.13 (m, 1H, NH_2), 2.02 (s, 3H, rimantadine), 1.79 – 1.42 (m, 12H, rimantadine), 1.31 (dd, $^3J_{HH}$ = 6.9, 4.5 Hz, 6H, CH(CH_3)$_2$), 1.23 (d, $^3J_{HH}$ = 6.7 Hz, 3H, rimantadine).^{13}C NMR (101 MHz, $CDCl_3$) δ 103.6 (*ipso-C* of *p*-cy), 96.3 (*ipso-C* of *p*-cy), 81.4 (*C*H-*p*-cy), 81.1 (*C*H-*p*-cy), 81.0 (*C*H-*p*-cy), 78.6 (*C*H-*p*-cy), 64.3, 38.1, 36.9, 36.7, 28.2, 13.8 (rimantadine), 31.3 (*C*H(CH$_3$)$_2$), 23.2 (CH(*C*H$_3$)$_2$), 21.7 (CH(*C*H$_3$)$_2$), 19.8 (*C*H$_3$of *p*-cy). Anal. Calc'd. $C_{22}H_{35}Br_2NRu{\cdot}0.5H_2O$: C, 45.29; H, 6.22; N, 2.40 Found: C, 45.24; H, 6.01; N, 2.42.

3. Results & discussion

3.1. Synthesis and NMR spectroscopy

The complexes (η^6-*p*-cy)Ru(NH$_2$R)Cl$_2$ (NH$_2$R = amantadine **(1),** memantine **(2)** and rimantadine **(3)**) and (η^6-*p*-cy)Ru(NH$_2$R)Br$_2$ (NH$_2$R = amantadine **(4)**, memantine **(5)** and rimantadine **(6)**) were synthesized by stirring [(η^6-*p*-cy)RuCl$_2$]$_2$ or [(η^6-*p*-cy)RuBr$_2$]$_2$,

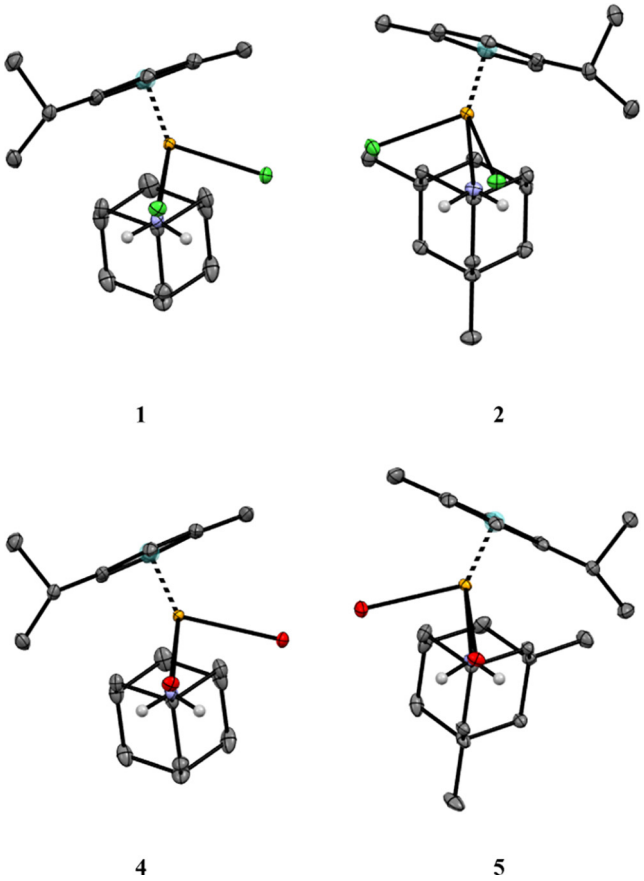

Fig. 6. Structures of amantadine and memantine complexes viewed along the N—C bond and bisecting the NH_2 bonds.

respectively, with excess amine in chloroform at room temperature. The complexes were isolated as orange solids in high purity and yield through precipitation. (Scheme 1, Fig. 2).

The identity of complexes **1**–**6** were confirmed by ^{1}H and $^{13}C\{^{1}H\}$ NMR spectroscopy in $CDCl_3$. The resonances for complexes **1**, **2**, **4**, and **5** include two doublets (aromatic methine, *p*-cymene ligand), a septet (aliphatic methine, *p*-cymene), a singlet (methyl, *p*-cymene), and a doublet (methyl, *p*-cymene) (Fig. 3). Spectroscopic differences between complexes **1**, **2**, **4**, and **5** and their synthetic precursors, $[(\eta^6\text{-}p\text{-cy})RuCl_2]_2$ and $[(\eta^6\text{-}p\text{-cy})RuBr_2]_2$, include deshielded *p*-cymene resonances and increased second order coupling effects (i.e., roofing) for the aromatic methines on the *p*-cymene. For complexes of the form $(\eta^6\text{-}p\text{-cymene})Ru(NH_2R)X_2$ (X = Cl, Br), the resonances associated with the *p*-cymene ligand are influenced by the halide on the complex (Fig. 3). For example, the septet for complex **1** is at 3.04 ppm while the septet for complex **4** is at 3.16 ppm. Resonances associated with the amine ligands are not as drastically impacted by the nature of the halide on the metal center. Similar resonances are observed when NMRs are obtained in DMSO d_6 (SI, Fig. S15 and S16), which indicates these species are stable in DMSO, the solvent used in cell viability studies (vide infra).

The ^{1}H NMR spectra of complexes **3** and **6** display additional resonances due to the chiral center on rimantadine. This chiral center causes the four aromatic methine hydrogens and the two isopropyl-methyl groups on the *p*-cymene ligand to be chemically inequivalent. (Fig. 4). For instance, in complex **3**, four resonances are observed for the methine hydrogens on the *p*-cymene ligand, instead of the two signals that are observed in complexes **1**, **2**, **4**, and **5**. These resonances appear as four doublets (5.43, 5.29, 5.28, and 5.16 ppm), with two doublets overlapping to resemble a triplet. The HSQC data (SI, Fig. S11) shows that each of these hydrogens correlate to a distinct carbon resonance. The HSQC data also confirms the presence of two distinct (diastereotopic) proton resonances for the NH_2 hydrogens on the rimantadine ligand, located at 3.20 and 2.09 ppm. Variable temperature NMR from 298 K to 318 K was conducted to confirm that the additional splitting in the aromatic protons was not due to hindered rotation of the *p*-cymene ring. No change in the ^{1}H NMR was observed (SI, Fig. S9) which confirms the additional resonances are due to the chiral center on the ligand.

3.2. X-ray crystallography analysis

To verify the identity of the synthesized complexes and identify their structural features, single crystal X-ray diffraction was performed on complexes **1**–**6**. The structures of the complexes are shown in Fig. 5. Potential rotation of the complexes' building blocks about certain bonds results in a variety of conformations of the complexes in this series. This is demonstrated in Fig. 6 for the amantadine and memantine complexes, which show variations in the rotation of the *p*-cymene ligand as it coordinates to Ru, the rotation about the Ru-N bond, and the rotation of the amantadine and memantine ligands about the N—C bond. This occurs in concert with different packing arrangements as the variations in the complexes (for example, the size of Br versus Cl, and the presence of methyl groups on memantine that are not present on amantadine) are introduced (Fig. 7). It is interesting to note that only in the

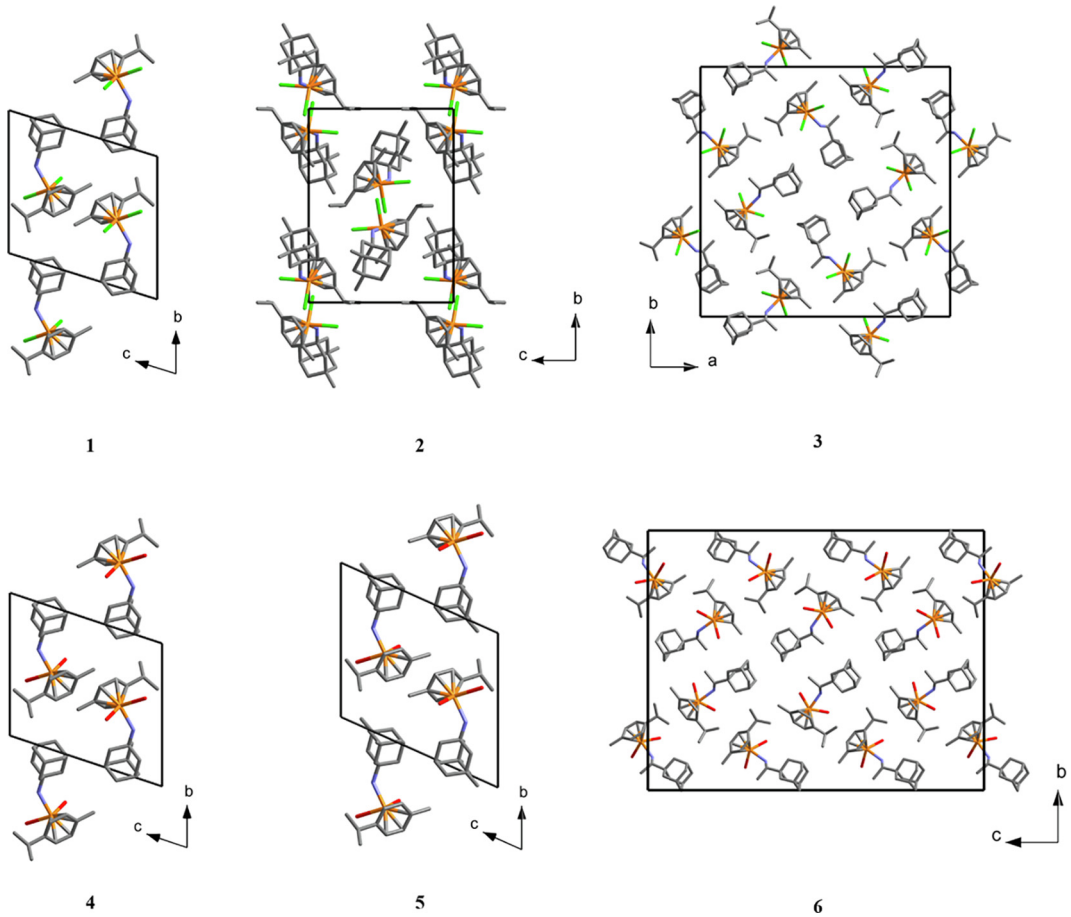

Fig. 7. Packing arrangements in complexes 1–**6**.

amantadine complexes **1** and **4** are the analogous chloride and bromide complexes isostructural. In the bromide series, the memantine complex **5** exhibits a similar packing motif to the amantadine complex **4** (and the complexes have similar lattice parameters), but it should be noted that there is a relative rotation about the Ru-N bond between the complexes (given a common NH_2-C orientation) that occurs to accomplish this. This leads to different intermolecular interactions.

The Ru-Cl bond lengths in **1**–**3** range from 2.405(5) Å to 2.4280 (5) Å, similar to those in related Ru-*p*-cymene complexes [21–26], and the Ru-Br bond lengths in **4**–**6** are, as expected, slightly longer, ranging from 2.5427(4) Å to 2.5653(2) Å. The distance from Ru to the centroid of the *p*-cymene ligand is consistent throughout this series (ranging from 1.669(2) Å to 1.683(2) Å in **1**–**6**), as are the Ru-N bond lengths (2.125(16) Å to 2.1761(11) Å), and these are also similar to related Ru-*p*-cymene complexes. The centroid-Ru-N angle ranges from 135.2(3)° to 136.1(2)° in the chloride complexes **1**–**3**, and from 132.5(2)° to 135.8(2)° in the bromide complexes **4**–**6**, perhaps indicating a slight steric influence of the larger bromide anions.

In the complexes, N—H···X and C—H···X (X = Cl, Br) hydrogen bonding both contribute to the intermolecular interactions that stabilize the long-range packing (SI, Table 2). In complex **1** (and the isostructural **4**), one amine hydrogen atom and one chlorine atom form hydrogen bonded dimers with their counterparts from a neighboring molecule (SI, Fig. S19). The second chlorine atom also extends the structure through a C—H···Cl interaction, where pairs of these interactions also form dimers between different neighboring molecules. Interactions involving *p*-cymene groups of neighboring molecules complete the three-dimensional framework of intermolecular interactions (SI, Fig. S20). These involve C—H···pi interactions between methyl hydrogen atoms and the aromatic core of a neighboring *p*-cymene group (H···C = 2.882 Å) as well as offset pi···pi interactions where the aromatic regions overlap (shortest C···C = 3.333 Å). In complex **2**, the Cl1 atom acts as a hydrogen bond acceptor for two different C—H···Cl interactions

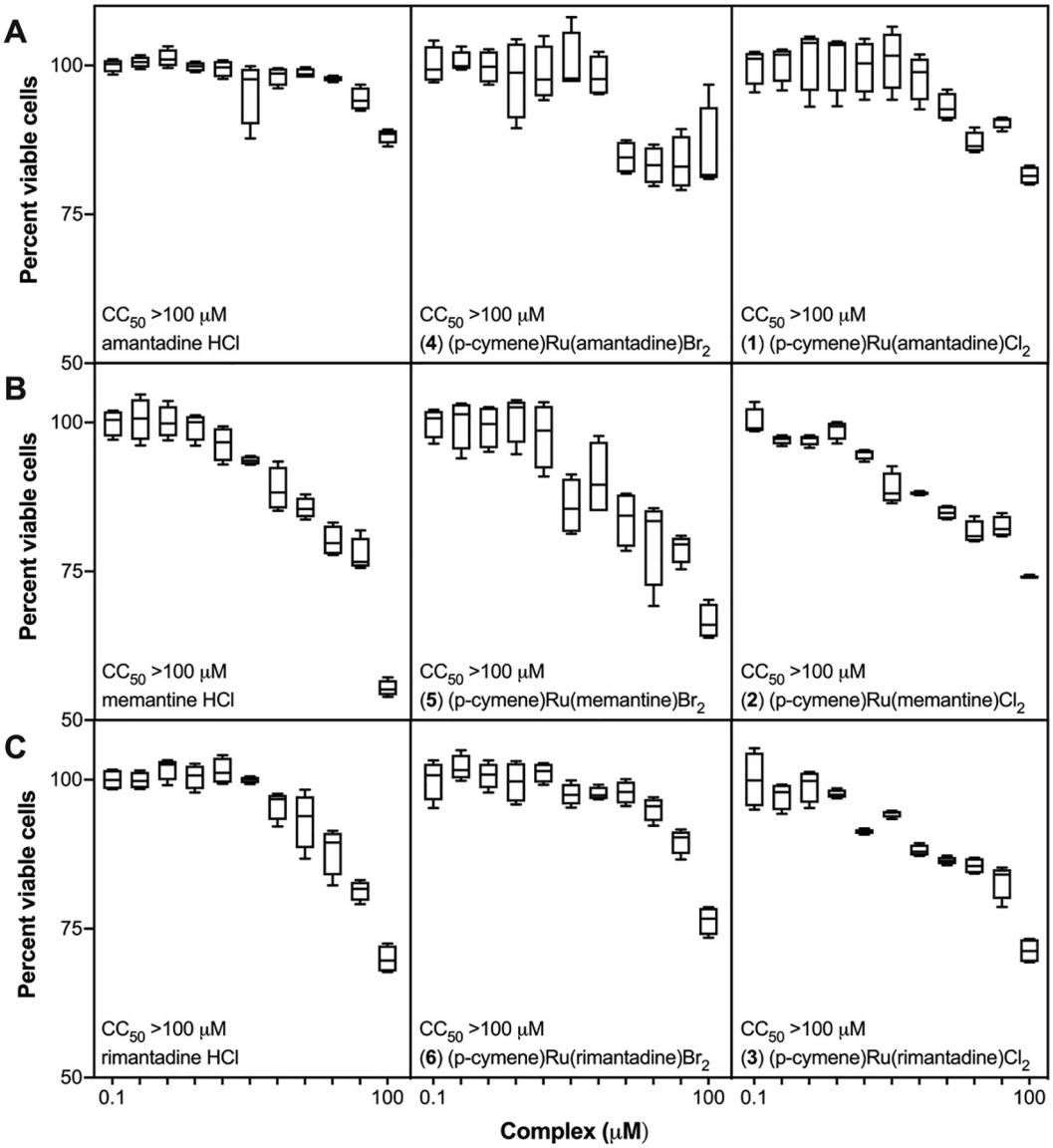

Fig. 8. Cell viability 24 h post-treatment with each complex. The amantadine, memantine, or rimantadine complexes and free ligands are grouped horizontally in A, B, and C, respectively. DBT-9 cells were treated with each complex over a series of two-fold dilutions beginning at 100 μM, with four replicates per concentration. Cell viability was determined using the CellTiter-Glo Assay. Luminescence values are shown normalized from 0 to 100%, and the box and whisker plots represent the 25th to 75th percentiles and min/max values, respectively.

to the memantine and *p*-cymene groups of two different neighboring molecules. Pairs of both of these interactions form separate dimers from a central molecule that extend the structure as chains of dimers (SI, Fig. S21). The *p*-cymene groups of neighboring molecules are not aligned for pi stacking interactions as they are in **1**, but they do support C—H···pi interactions involving the hydrogen atoms of methyl groups of two different neighboring molecules (one from a neighboring *p*-cymene group (H···C = 2.863 Å) and the other from a neighboring memantine group (H···C = 2.892 Å) to extend the structure in three dimensions. Likewise, complex **3** does not feature amine hydrogen bonding, but does again rely on dimers of C—H···Cl hydrogen bonds to extend the structure in one dimension along the *c*-axis. This time the dimers involve both chlorine atoms of one molecule and two hydrogen atoms from the aromatic core of the *p*-cymene group of a neighboring molecule (SI, Fig. S22). In **5**, the shortest hydrogen bonding contact to the bromine atoms again occurs through a CH_2 group of the memantine group, and pairs of these C—H···Br interactions form dimers (Fig. S23). Unlike **2**, where additional dimers were formed by C—H···Cl interactions to the same chlorine atom, the additional C—H···Br dimers in **5** are formed through the second bromine atom. This is more similar to what occurred in **1** and **4**, where this bromine atom interacts with a hydrogen atom of a neighboring *p*-cymene group. This creates a one-dimensional motif. The pi interactions in **5**, however, are much less pronounced than in **1** and **4**. While the *p*-cymene groups are still aligned for a potential offset pi···pi interaction, the shortest C···C contact occurs at a much longer distance (3.755 Å). In this way the pi···pi and C—H···X interactions involving the *p*-cymene group appear to have a more cooperative effect in **1** and **4** than in **5**. Finally, complex **6** features similar intermolecular interactions to **3**, where in **6** the two bromine atoms of a given molecule interact with two hydrogen atoms on the aromatic core of the *p*-cymene group of a neighboring molecule to produce one-dimensional chains. There are three such unique chains in the structure, corresponding to the three unique molecules in the asymmetric unit. While the molecules all have different orientations relative to one another, all of these chains propagate along the *a*-axis via the C—H···Br interactions (SI, Fig. S24).

3.3. Cell viability studies

To determine the effect of complexes **1**–**6** or their free ligands on cell viability, DBT-9 cells were treated with two-fold dilutions of each complex or free ligand, and cell viability was measured 24 h post-treatment. Complexes **1**–**6** and their free ligands all have 50% cytotoxic concentrations (CC_{50}) above 100 μM (Fig. 8), though the CC_{50} for memantine is likely close to 100 μM1 in DBT-9 cells. Additionally, neither the chlorine nor bromine *p*-cymene ruthenium(II) complexes significantly changed the concentration-dependent cytotoxicity of the bioactive free ligand, at least out to the concentrations tested. Concentrations above 100 μM were not tested, as DMSO can begin to impact cell viability at 0.5% (v/v) or above. The CC_{50} values for amantadine, rimantadine, and memantine are cell-type specific, but are generally reported to be around or greater-than 100 μM [31–33]. The CC_{50} for amantadine in several eukaryotic cell lines, including human-derived lines, ranges from approximately 95 to 850 μM [31]. CC_{50} values of greater than 100 μM have been reported for rimantadine [32] and memantine [33] in canine or murine cells, respectively, though exact CC_{50} values were not provided. Together, these data indicate that complexation of these three bioactive ligands to ruthenium(II) centers does not significantly enhance cellular toxicity. Future studies assessing potential antiviral activity will be needed to determine whether these CC_{50} values are sufficient to obtain an acceptable selectivity index.

4. Conclusions

Six new ruthenium(II) complexes containing bioactive ligands were synthesized and characterized by NMR spectroscopy and X-ray crystallography. Derivatives of (*p*-cymene)$RuCl_2$ containing other extended amines have been previously characterized by X-ray crystallography, with the amantadine, memantine, and rimantadine derivatives here serving as new structural additions to this family. The characterization of (*p*-cy)$RuBr_2$ analogs reported in this study are novel, and, in some cases, the Br-analogs display packing arrangements that deviate from that of their Cl-congeners. Initial cell viability studies indicate that complexation of these three bioactive ligands to ruthenium(II) centers does not significantly enhance cellular toxicity compared to their respective free ligands. Furthermore, these studies provide a suitable window of concentrations at which to test potential antiviral activity and to determine whether these complexes have a tolerable selectivity index.

CRediT authorship contribution statement

Sarah L. McDarmont: Investigation, Validation, Formal analysis, Writing - original draft, Writing - review & editing. **Meredith H. Jones:** Investigation, Formal analysis, Writing - review & editing. **Colin D. McMillen:** Methodology, Investigation, Formal analysis, Resources, Visualization, Writing - original draft, Writing - review & editing. **Everett Clinton Smith:** Investigation, Formal analysis, Writing - original draft, Writing - review & editing, Visualization, Funding acquisition. **Jared A. Pienkos:** Conceptualization, Methodology, Investigation, Formal analysis, Resources, Writing - original draft, Writing - review & editing, Funding acquisition. **Evan E. Joslin:** Project administration, Methodology, Investigation, Formal analysis, Visualization, Resources, Writing - original draft, Writing - review & editing, Funding acquisition.

Declaration of Competing Interest

The authors declare that they have no known competing financial interests or personal relationships that could have appeared to influence the work reported in this paper.

Acknowledgements

E.E.J and J.A.P would like to thank all the undergraduate students listed for their hard work. E.E.J and E.C.S would like to thank The University of the South for financial support. J.A.P would like to thank the University of Tennessee at Chattanooga's faculty grants committee for funding.

Appendix A. Supplementary data

CCDC deposition numbers 2055507-2055513 contains the supplementary crystallographic data for complexes **1–6** and **2**·**2CHCl$_3$**. These data can be obtained free of charge via http://www.ccdc.cam.ac.uk/conts/retrieving.html or from the Cambridge Crystallographic Data Center, 12 Union Road, Cambridge CB2 1EZ, UK; fax: (+44) 1223-336-033; or email: deposit@ccdc.cam.ac.uk. Supplementary data to this article can be found online at https://doi.org/10.1016/j.poly.2021.115130.

References

[1] R.E.F. de Paiva, A. Marçal Neto, I.A. Santos, A.C.G. Jardim, P.P. Corbi, F.R.G. Bergamini, What is holding back the development of antiviral metallodrugs? a literature overview and implications for SARS-CoV-2 therapeutics and future viral outbreaks, Dalton Trans. 49 (45) (2020) 16004–16033, https://doi.org/10.1039/D0DT02478C.

[2] S. Dasari, P. Bernard Tchounwou, Cisplatin in cancer therapy: molecular mechanisms of action, Eur. J. Pharmacol. 740 (2014) 364–378, https://doi.org/10.1016/j.ejphar.2014.07.025.
[3] I. Ott, R. Gust, Non platinum metal complexes as anti-cancer drugs, Arch. Pharm. Chem. Life Sci. 340 (3) (2007) 117–126, https://doi.org/10.1002/ardp.200600151.
[4] K. Seiji, C. Angela, Next-generation anticancer metallodrugs, Curr. Top. Med. Chem. 12 (3) (2012) 219–235.
[5] C.S.K. Rajapakse, A. Martínez, B. Naoulou, A.A. Jarzecki, L. Suárez, C. Deregnaucourt, V. Sinou, J. Schrével, E. Musi, G. Ambrosini, G.K. Schwartz, R. A. Sánchez-Delgado, Synthesis, characterization, and in vitro antimalarial and antitumor activity of new ruthenium(II) complexes of chloroquine, Inorg. Chem. 48 (3) (2009) 1122–1131, https://doi.org/10.1021/ic802220w.
[6] M. Carcelli, A. Bacchi, P. Pelagatti, G. Rispoli, D. Rogolino, T.W. Sanchez, M. Sechi, N. Neamati, Ruthenium arene complexes as HIV-1 integrase strand transfer inhibitors, J. Inorg. Biochem. 118 (2013) 74–82.
[7] A. Bacchi, M. Carcelli, C. Compari, E. Fisicaro, N. Pala, G. Rispoli, D. Rogolino, T. W. Sanchez, M. Sechi, V. Sinisi, N. Neamati, Investigating the role of metal chelation in HIV-1 integrase strand transfer inhibitors, J. Med. Chem. 54 (24) (2011) 8407–8420, https://doi.org/10.1021/jm200851g.
[8] C.N. Banti, N. Kourkoumelis, A.G. Hatzidimitriou, I. Antoniadou, A. Dimou, M. Rallis, A. Hoffmann, M. Schmidtke, K. McGuire, D. Busath, A. Kolocouris, S.K. Hadjikakou, Amantadine copper(II) chloride conjugate with possible implementation in influenza virus inhibition, Polyhedron 185 (2020) 114590, https://doi.org/10.1016/j.poly.2020.114590.
[9] N. Cimolai, Potentially repurposing adamantanes for COVID-19, J Med Virol 92 (6) (2020) 531–532, https://doi.org/10.1002/jmv.25752.
[10] C. Wang, K. Takeuchi, L.H. Pinto, R.A. Lamb, Ion channel activity of influenza A virus M2 protein: characterization of the amantadine block, J. Virol. 67 (9) (1993) 5585.
[11] D. Schoeman, B.C. Fielding, Coronavirus envelope protein: current knowledge, Virol. J. 16 (1) (2019) 69.
[12] H.R. Payne, J. Storz, W.G. Henk, Initial events in bovine coronavirus infection: analysis through immunogold probes and lysosomotropic inhibitors, Arch. Virol. 114 (3-4) (1990) 175–189, https://doi.org/10.1007/BF01310747.
[13] J.L. Leibowitz, S.J. Reneker, The effect of amantadine on mouse hepatitis virus replication, Adv. Exp. Med. Biol. 342 (1993) 117–122.
[14] F. Chen, K.H. Chan, Y. Jiang, R.Y. Kao, H.T. Lu, K.W. Fan, V.C. Cheng, W.H. Tsui, I. F. Hung, T.S. Lee, Y. Guan, J.S. Peiris, K.Y. Yuen, In vitro susceptibility of 10 clinical isolates of SARS coronavirus to selected antiviral compounds, J. Clin. Virol. 31 (1) (2004) 69–75.
[15] E. Brison, H. Jacomy, M. Desforges, P.J. Talbot, Novel treatment with neuroprotective and antiviral properties against a neuroinvasive human respiratory virus, J. Virol. 88 (3) (2014) 1548–1563, https://doi.org/10.1128/JVI.02972-13.
[16] J.A. Tanner, B.-J. Zheng, J. Zhou, R.M. Watt, J.-Q. Jiang, K.-L. Wong, Y.-P. Lin, L.-Y. Lu, M.-L. He, H.-F. Kung, A.J. Kesel, J.-D. Huang, The adamantane-derived bananins are potent inhibitors of the helicase activities and replication of SARS coronavirus, Chem. Biol. 12 (3) (2005) 303–311, https://doi.org/10.1016/j.chembiol.2005.01.006.
[17] T. Takano, K. Nakano, T. Doki, T. Hohdatsu, Differential effects of viroporin inhibitors against feline infectious peritonitis virus serotypes I and II, Arch. Virol. 160 (5) (2015) 1163–1170, https://doi.org/10.1007/s00705-015-2370-x.
[18] W.L. Davies, R.R. Grunert, R.F. Haff, J.W. McGahen, E.M. Neumayer, M. Paulshock, J.C. Watts, T.R. Wood, E.C. Hermann, C.E. Hoffmann, Antiviral activity of 1-adamantanamine (amantadine), Science 144 (3620) (1964) 862–863, https://doi.org/10.1126/science:144.3620.862.
[19] J. Kornhuber, M. Weller, K. Schoppmeyer, P. Riederer, Amantadine and memantine are NMDA receptor antagonists with neuroprotective properties, J. Neural Transm. Suppl. 43 (1994) 91–104.
[20] S.M. Wintermeyer, M.C. Nahata, Rimantadine: a clinical perspective, Ann. Pharmacother. 29 (3) (1995) 299–310, https://doi.org/10.1177/106002809502900312.
[21] C. Binnani, D. Tyagi, R.K. Rai, S.M. Mobin, S.K. Singh, C–H bond activation/arylation catalyzed by arene–ruthenium–aniline complexes in water, Chemistry – Asian J. 11 (21) (2016) 3022–3031.
[22] J. Grau, V. Noe, C. Ciudad, M.J. Prieto, M. Font-Bardia, T. Calvet, V. Moreno, New π-arene ruthenium(II) piano-stool complexes with nitrogen ligands, J. Inorg. Biochem. 109 (2012) 72–81.
[23] P. Govindaswamy, Y.A. Mozharivskyj, M.R. Kollipara, New neutral and cationic η6-arene ruthenium complexes with phosphine and amine ligands: syntheses and molecular structures of $[(\eta^6\text{-}p\text{-cymene})Ru(NH_2CH_2C_6H_5)Cl_2]$, $[(\eta^6\text{-}C_6Me_6)Ru(PPh_2Py)Cl_2]$ and $[(\eta^6\text{-}C_6Me_6)Ru(PPh_2Py)Cl]^+$, Polyhedron 23 (18) (2004) 3115–3123.
[24] R. Marsh, Space group Cc: an update, Acta Crystallogr. Section B 60 (2) (2004) 252–253.
[25] M.J. Begley, S. Harrison, A.H. Wright, Dichloro(*p*-cymene)(*p*-toluidine) ruthenium(II), Acta Crystallogr. Section C 47 (2) (1991) 318–320.
[26] M. Nirmala, M. Adinarayana, K. Ramesh, M. Maruthupandi, M. Vaddamanu, G. Raju, G. Prabusankar, Water-soluble superbulky (η^6-*p*-cymene) ruthenium(II) amine: an active catalyst in the oxidative homocoupling of arylboronic acids and the hydration of organonitriles, New J. Chem. 42 (18) (2018) 15221–15230.
[27] M.G. Mendoza-Ferri, C.G. Hartinger, A.A. Nazarov, R.E. Eichinger, M.A. Jakupec, K. Severin, B.K. Keppler, Influence of the arene ligand, the number and type of metal centers, and the leaving group on the in vitro antitumor activity of polynuclear organometallic compounds, Organometallics 28 (21) (2009) 6260–6265.
[28] APEX 3, Bruker-AXS Inc., Madison, WI, 2015.
[29] G. Sheldrick, Crystal structure refinement with SHELXL, Acta Crystallogr. Section C 71 (1) (2015) 3–8.
[30] W. Chen, R.S. Baric, Molecular anatomy of mouse hepatitis virus persistence: coevolution of increased host cell resistance and virus virulence, J. Virol. 70 (6) (1996) 3947–3960.
[31] Y. Furuta, K. Takahashi, Y. Fukuda, M. Kuno, T. Kamiyama, K. Kozaki, N. Nomura, H. Egawa, S. Minami, Y. Watanabe, H. Narita, K. Shiraki, In vitro and in vivo activities of anti-influenza virus compound T-705, Antimicrob. Agents Chemother. 46 (4) (2002) 977–981.
[32] A. Drakopoulos, C. Tzitzoglaki, K. McGuire, A. Hoffmann, A. Konstantinidi, D. Kolokouris, C. Ma, K. Freudenberger, J. Hutterer, G. Gauglitz, J. Wang, M. Schmidtke, D.D. Busath, A. Kolocouris, Unraveling the binding, proton blockage, and inhibition of influenza M2 WT and S31N by rimantadine variants, ACS Med. Chem. Lett. 9 (3) (2018) 198–203.
[33] H.F. Santos Souza, S.C. Rocha, F.S. Damasceno, L.N. Rapado, E.M.F. Pral, C.R.F. Marinho, A.M. Silber, The effect of memantine, an antagonist of the NMDA glutamate receptor, in in vitro and in vivo infections by Trypanosoma cruzi, PLoS Negl. Trop. Dis. 13 (9) (2019) e0007226.